

Direct Imaging of Polyethylene Films at Single-Chain Resolution with Torsional Tapping Atomic Force Microscopy

Nic Mullin and Jamie K. Hobbs*

Department of Physics and Astronomy, University of Sheffield, Hounsfield Road, United Kingdom S3 7RH

(Received 7 July 2011; published 4 November 2011)

The physical properties of semicrystalline polymers depend on the organisation of chains within the crystal and amorphous regions, on the interface between the two, and on the location and nature of defects. Here, torsional tapping atomic force microscopy has been used to image crystalline lamellae and the crystal–amorphous-region interface at the single-chain level with resolution down to 3.7 Å. Defects within the crystalline phase, such as buried folds and chain ends, are revealed. Imaging at the chain level also allows direct measurement of crystalline stem lengths, providing a potential route to test theories of crystal thickness selection.

DOI: 10.1103/PhysRevLett.107.197801

PACS numbers: 61.41.+e, 07.79.Lh, 64.70.dg

In semicrystalline polymers the crystal structure, defects within the crystalline lamellae, and the nature of the interface between the crystal and amorphous regions play a central role in determining the ultimate material properties [1]. Over the past 50 years there has been extensive debate and theoretical development on the physical processes that occur during polymer crystallization. Fundamental questions such as “why are crystals thinner than expected from equilibrium thermodynamics?” “How do chains fold back to reenter the same crystal?” and “What role is played by “loose loops” and “tie chains” in mechanical properties of bulk films?” still await definitive answers [2–9]. A lack of direct imaging data at the molecular scale makes it difficult to reach a consensus on these issues which are at the heart of our understanding of this important class of materials. Here we show that a new atomic force microscopy (AFM) technique, torsional tapping AFM (TTAFM) [10], is capable of obtaining the necessary resolution even on rough and soft surfaces in air. Utilizing TTAFM with carbon whisker tips [11] we directly visualize individual chains in the crystalline lattice of polyethylene down to 3.7 Å resolution in air under ambient conditions. By selection of suitable imaging conditions we are able to image loose molecular loops at the crystal–amorphous-region interface, the existence of a tight adjacent fold buried on the crystal surface, and to obtain the chain-by-chain statistics of crystal stem length that are a potential output of growth models [12].

Existing high resolution microscopy techniques typically require samples to be very thin films (TEM, STEM) [13], close to atomically flat (AFM) [14,15], and conducting in the case of scanning tunnelling microscopy (STM). AFM has the fewest constraints on sample preparation, but sub-nm resolution is not routine. Lattice resolution can be obtained in contact mode [16], but this has revealed limited new information. In all but a few exceptional cases [17,18] true molecular resolution has only been obtained using dynamic modes of operation either in ultrahigh vacuum [19,20], or under liquid [21–23], removing the strong and

nonspecific attractive force that comes from the water meniscus that forms between the tip and the sample under ambient conditions.

In oscillatory modes of AFM the sensitivity of the measurement of force gradient, and hence the ultimate resolution obtainable, depends on the dynamics of the oscillating cantilever [20] and the noise associated with detecting the cantilever response [23]. Torsionally oscillated T-shaped cantilevers [Fig. 1(a)] have improved dynamics compared to conventional beam shaped cantilevers [10], and also provide a higher signal-to-noise ratio for a given amplitude due to the relatively small offset of the tip from the torsion axis of the cantilever, increasing the

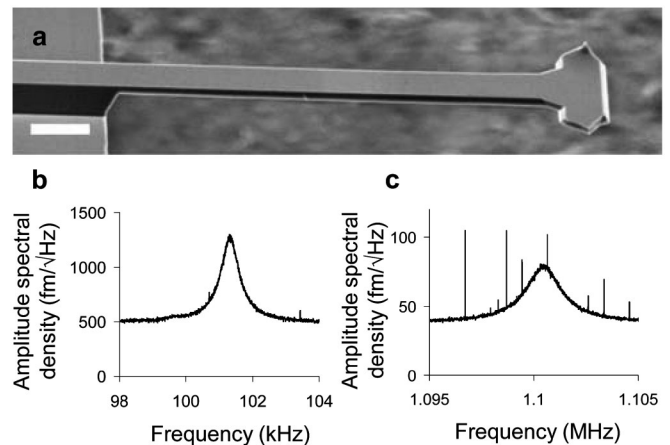


FIG. 1. (a) Scanning electron micrograph of a Mikromasch TL01 cantilever. Scale bar 20 μm . (b) Flexural thermal noise spectrum around the first flexural resonance (resonant frequency ~ 101 kHz, quality factor ~ 280) of a TL01 cantilever. The deflection noise floor is taken to be the baseline around the resonant peak; 512 $\text{fm}/\sqrt{\text{Hz}}$. (c) Torsional thermal noise spectrum around the first torsional resonance (resonant frequency ~ 1.1 MHz, quality factor ~ 900) of the same TL01 cantilever as in Fig. 1(b), taken on the same AFM with the same laser alignment. The noise floor is 40 $\text{fm}/\sqrt{\text{Hz}}$.

optical lever sensitivity. Both of these factors lead to increased force sensitivity. Figures 1(b) and 1(c) show the measured deflection noise in both the torsional and flexural axes, showing an approximately 12 fold improvement in torsion compared to flexion on an otherwise identical experimental setup. As it is the properties of the torsional bending mode that control the cantilever dynamics, the vertical (flexural) stiffness of the cantilever can be kept relatively low, reducing the force between tip and surface when the AFM feedback has to run with a high error signal, for example, on rough surfaces. The combination of enhanced sensitivity and reduced forces when feedback error occurs mean that ultrasharp, “whisker” tips [11] can be used with lower risk of tip blunting.

We have applied this new technology to image high density polyethylene as it provides an exceptionally well-studied model system for polymer crystallization. Polyethylene (PE) ($M_w = 169$ kDa, $M_w/M_n = 1.52$, Fluka) was purchased from Sigma Aldrich and used without further purification. Samples were made by dissolving PE in paraxylene (Sigma Aldrich) at a concentration of 1% by mass at 135 °C, then placing a droplet of hot solution onto a glass slide on a hot stage (Linkam TP94) at 160 °C and holding for 5 minutes to allow the solvent to evaporate. The sample was then cooled to 135 °C and the surface was sheared with a razor blade to orient the film. This gave films of varying thickness, typically of the order of several tens of microns. After shearing, the sample was held at 135 °C for a further 3 minutes before either crystallising on quenching to room temperature on a metal block or on cooling from 135 °C at 1 °C/min to 100 °C before quenching to room temperature.

All imaging was carried out in air at ambient room temperature using a Multimode AFM, equipped with a

J-scanner, NanoScope IIIa controller and Basic Extender (Veeco Instruments, California, USA). T-shaped cantilevers (TL01 Hi’Res-C, Mikromasch) with carbon whisker tips were driven into torsional oscillation using a home built cantilever holder. The torsional drive is supplied by bonding the cantilever chip onto a “see-saw” comprised of two small ($4 \times 1.5 \times 0.5$ mm), oppositely-poled piezoelectric actuators (cut from PQYY + 0346 piezoelectric elements, Physik Instrumente) joined by a glass rocker. The actuators are then driven by the same sinusoidal drive signal (the signal usually used for tapping mode excitation) to provide a rocking motion. Torsional cantilever oscillations were detected by interchanging the signal from the top right and bottom left photodiode quadrants, resulting in the lateral (torsional) deflection signal being treated by the AFM as if it were the vertical (flexural) signal. Optimal imaging conditions were obtained with free amplitudes of 10–15 nm, set points >95% of the free amplitude and scan rates of 1.5–2 Hz. In the absence of feedback error signal, these parameters (combined with the quality factor) allow the average tip-sample force to be estimated [24] as approximately 78 pN, resulting in a peak repulsive force somewhat higher than this value. Height and phase [25] images were captured simultaneously and flattened or plane-fitted (to first order in both cases) where necessary using NanoScope (Version 5.3, Revision 3) or Gwyddion software, which was also used for measurements and analysis.

The simple extension process applied to the molten film provides a polymer surface with crystals having a well defined orientation [26]. The lamellae are perpendicular to the extension axis, and hence their thin dimension, which is a vertical section through each lamellar crystal, lies in the plane of the surface. Figure 2(a) is an overview

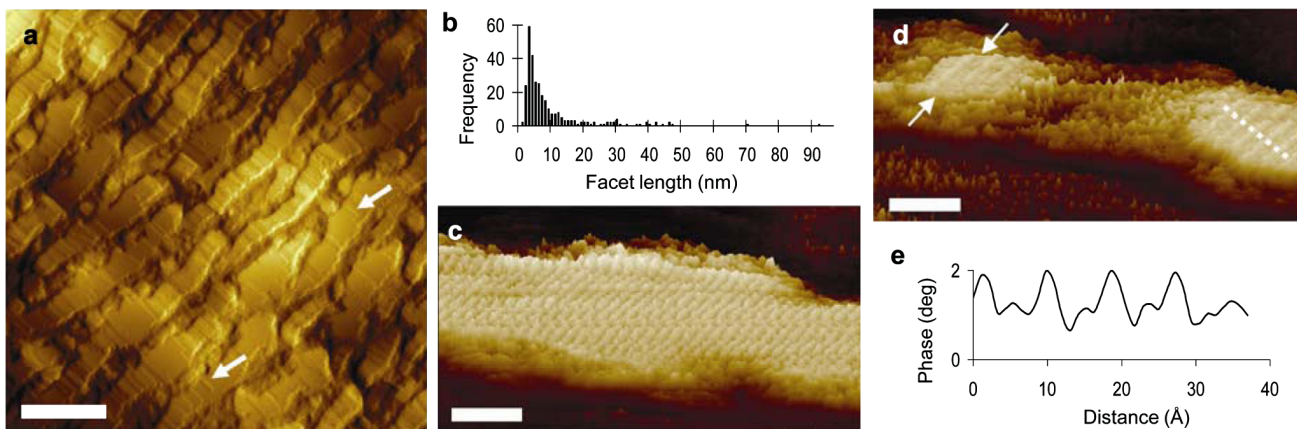


FIG. 2 (color online). (a) Overview of a sheared polyethylene film. The shearing direction is along the diagonal from bottom right to top left. Height image, lit from the side in order to delineate the facets. Scale bar 100 nm. (b) Histogram of the lengths of facets on the lamella surface measured from Fig. 2(a). (c) High resolution phase image showing the (110) surface of a crystalline polyethylene lamella. The image is rendered in pseudo-3d, black to white scale 10° . Scale bar 5 nm. (d) High resolution phase image of a lamella whose the surface corresponds to the (010) plane of the polyethylene crystal. The image is rendered in pseudo 3d, black to white scale 10° . Scale bar 5 nm. (e) Cross-section along the dotted line on Fig. 2(d). The lower peaks are due to the central chain in the unit cell. The cross-section is averaged over 17 lines parallel with the dotted line indicated.

showing multiple oriented lamellae. In the samples imaged the amorphous region is typically 3–10 nm below the crystalline regions, this height variation occurring over lateral distances of ~ 10 nm. The multiply faceted and stepped nature of the crystal surfaces is immediately clear, with step heights of typically ~ 4 Å corresponding to the spacing between adjacent (110) planes. Previous AFM studies of polymer crystal edge surfaces typically see rounded or even nodular surfaces to the lamellae. This may be due to tip convolution artefacts, the extremely sharp and high aspect ratio tips used here revealing the true structure. All of the crystal lamellae contain pronounced step edges, separated by flat regions [several nanometers up to tens of nanometers, Fig. 2(b)] in a manner akin to a classical, small molecule crystal. This stepped surface may not reflect the state of the crystal surface during growth [9], but similarly it does not have the appearance of surface that has reorganized extensively. Under the crystallization conditions used here (rapid quenching) there is a continuous distribution of distances between step edges.

Figures 2(c) and 2(d) show high resolution phase images of lamellae with different orientations of their crystallography relative to the surface. Single chains are resolved, and both the (110), Fig. 2(c), and (010), Fig. 2(d), surfaces can be identified. The (110) surface is the densely packed crystal plane and the most common growth front plane, so it is not unexpected that this is observed, and is seen on most of the lamellae that we have imaged. The (010) is a fast growing plane, so is most probably seen due to the influence of the free surface, forestalling growth. The (010) is the least densely packed low index face, and the individual chains are clearly visible in both phase [Fig. 2(d)] and height (not shown). In the phase image a faint line (arrows) is apparent between the two chains, which is believed to be the central chain in the unit cell. The lateral separation between this chain and its neighbor is known to be 3.69 Å (from x-ray scattering), indicating the resolution obtained. The images presented here have not been corrected for drift and the microscope scanner is open loop, so precise measurements of distances cannot be made.

In Fig. 2(a) there are a number of cases where crystalline chains at the surface do not span the full width of the underlying layer (arrows). Figure 3(a) shows a higher resolution image of a step edge which includes a chain that does not span the entire crystal thickness. Here a sharp fold in the chain is visible (arrow) as it bends back to enter the adjacent lattice site. The nature of “chain folding” in polymers has been discussed for many years [3]. Here the fold is sharp and tight, with a length between adjacent crystalline units of approximately 8 Å corresponding to ~ 6 carbon-carbon bonds. However, the conformation observed here may not be indicative of the bulk of the chains that exit at the basal planes of the lamellae. The energetic penalty associated with a loose fold is greater for

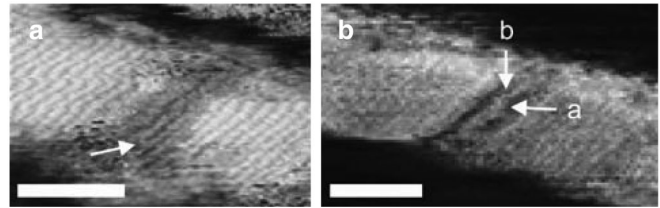


FIG. 3. (a) High resolution phase image showing a chain that folds and reenters the crystal before reaching the edge of the lamella (arrow). Black to white scale 18° . Scale bar 5 nm. (b) High resolution phase image showing a chain whose end has deposited in the center of a lamella. Black to white scale 15° . Scale bar 5 nm.

a chain that folds back before reaching the crystal surface, and the free surface constrains the chain to two dimensions, introducing some bias. However, it is clear that tight folds do exist in thick as well as monolayer [27] films. Figure 3(b) shows a chain in which the chain end (arrow a) has deposited near to the center of the crystal. This introduces a defect, in this case causing a kink (arrow b) in the chain as the chain end is bypassed.

The mechanical properties of semicrystalline polymers are strongly influenced by the nature of the crystal/amorphous-region interface. From our data it is apparent that the crystal thickness, when measured on a chain-by-chain basis [Fig. 4(a)], is not a constant for each lamella. The distribution is quite symmetric, and variations in stem length of 20% from the mean are not uncommon in the 312 chains measured. These data have several implications for our understanding of polymer crystals. First, this variation is a real variation in the measured length of the ordered chain, and that order is stable over the (several minute) timescale of obtaining an image, despite any chain diffusion processes occurring at this temperature [28]. Second, variations in crystal thickness suggested by ex-

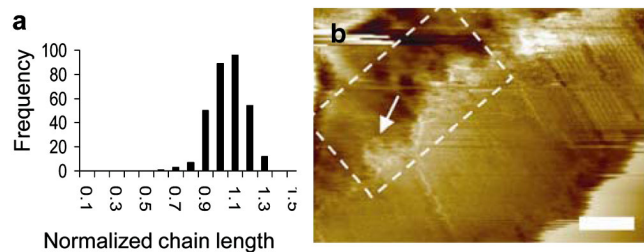


FIG. 4 (color online). (a) Histogram of crystalline chain lengths (normalized to the mean thickness of their respective lamellae to remove issues with drift) measured from individual chains visible in 3 different lamellae. The bin width corresponds to ~ 6 Å. (b) Phase image showing the interface between the edge of a crystalline lamella and the amorphous phase. Chains in the (010) surface of the crystal are resolved at the top right of the frame. The upper surface of the central region of the lamella is believed to be the (110), which is not resolved here. Free loops emanating from the fold surface project into the amorphous region (dashed box). Black to white scale 25° . Scale bar 10 nm.

periments on crystal stability [29], and by simulations [7–9], are observed directly at the chain level. The slight skewing of the distribution may be a result of the crystallization occurring on cooling, and so the initial crystal thickness is likely to be thicker than the minimum stable thickness, biasing chain deposition slightly towards shorter lengths [12]. The observed variations in thickness might lead to the differences in melting temperature that are commonly seen for apparently homogeneous polymer samples, the longer crystalline chain portions acting as nucleation sites for crystal thickening when the sample is annealed close to its melting temperature. Steps in thickness of up to a nanometer (eight CH₂ units) are observed, and this roughness will also influence the local level of chain constraint, as monitored by spectroscopy methods. Crystallization during slow cooling [as in Fig. 4(b)] does not result in a smoother crystal surface, implying that the energy penalty associated with this roughness is small.

Figure 4(b) shows a high magnification image of the interface between a crystal and the surrounding amorphous region. Here the scan parameters have been optimized for imaging the amorphous region, revealing individual chains as they exit and reenter the crystal (dashed box). These loops project up to ~5 nm into the surrounding amorphous material, and in one case two loops appear knotted together (arrow). That the chains can still be imaged within the amorphous phase, more than 100 °C above the T_g of polyethylene, implies a high degree of constraint, coming from the pinning of the loop at its ends in the crystal surface. Such a “rigid” amorphous phase has been found with spectroscopy studies [30], which give a relaxation time similar to though faster than that of the crystalline component [31], and is here confirmed by direct imaging. Additional constraint may also be placed on the chains by the presence of the free surface, and associated surface and capillary forces (from surface water). However, such chain resolution is only obtained close to the crystal, so the crystal–amorphous-region interface is at least partly responsible.

In summary, we have directly imaged crystal structure down to 3.7 Å resolution on the surface of a bulk polymer film under ambient conditions using torsional tapping AFM. Previous studies have obtained chain resolution in monolayer films [27,32], but TTAfM provides the capability to obtain such resolution on thick samples with a roughness seen under conventional processing conditions. Imaging both crystal defects and amorphous chains, apparently tightly constrained by their connection to the neighboring crystal, reveals a high degree of disorder, while the crystal surface is shown to be sharply stepped in agreement with classical theory. In the development of TTAfM we have found that each improvement in signal-to-noise provides a concomitant improvement in resolution. The instrument used to obtain this data was a standard AFM, without specialized optics or electronics.

Improvements already made in this direction [23], should provide further enhancements to the resolution obtainable by torsional tapping AFM on these soft materials, and potentially the attainment of similar resolution on more disordered samples (e.g., polymer glasses).

We thank the EPSRC UK for funding. We thank Prof Wenbing Hu, Nanjing University, China, and Dr Simon Hanna, University of Bristol, UK, for helpful discussions.

*Corresponding author.

Jamie.hobbs@sheffield.ac.uk.

- [1] G.R. Strobl, *The Physics of Polymers: Concepts for Understanding Their Structures and Behaviours* (Springer, New York 2007).
- [2] A. Keller, *Philos. Mag.* **2**, 1171 (1957).
- [3] *Faraday Discuss. Chem. Soc.* **68** (1979).
- [4] D.C. Bassett, *Principles of Polymer Morphology* (Cambridge University Press, Cambridge, England, 1981).
- [5] B. Wunderlich, *Macromolecular Physics: Crystal Nucleation, Growth, Annealing* (Academic Press, Waltham, 1976), Vol. 2.
- [6] S. Rastogi *et al.*, *Nature Mater.* **4**, 635 (2005).
- [7] W.-B. Hu, D. Frenkel and V.B.F. Mathot, *Macromolecules* **36**, 8178 (2003).
- [8] P. Welch and M. Muthukumar, *Phys. Rev. Lett.* **87**, 218302 (2001).
- [9] C. Luo and J-U. Sommer, *Macromolecules* **44**, 1523 (2011).
- [10] N. Mullin *et al.*, *Appl. Phys. Lett.* **94**, 173109 (2009).
- [11] D. Klinov and S. Magonov, *Appl. Phys. Lett.* **84**, 2697 (2004).
- [12] J.P.K. Doye, *Polymer* **41**, 8857 (2000).
- [13] D.B. Williams and C.B. Carter, *Transmission Electron Microscopy A Textbook for Materials Science* (Springer, New York 2009).
- [14] Y. Gan, *Surf. Sci. Rep.* **64**, 99 (2009).
- [15] C. Barth *et al.*, *Adv. Mater.* **23**, 477 (2011).
- [16] G. Binnig *et al.*, *Europhys. Lett.* **3**, 1281 (1987).
- [17] D.J. Muller and A. Engel, *Curr. Opin. Colloid Interface Sci.* **13**, 338 (2008).
- [18] S. Scheuring and J.N. Sturgis, *Photosynth. Res.* **102**, 197 (2009).
- [19] F.J. Giessibl *et al.*, *Science* **289**, 422 (2000).
- [20] T.R. Albrecht *et al.*, *J. Appl. Phys.* **69**, 668 (1991).
- [21] T. Fukuma, M.J. Higgins, and S.P. Jarvis, *Phys. Rev. Lett.* **98**, 106101 (2007).
- [22] B.W. Hoogenboom *et al.*, *Appl. Phys. Lett.* **88**, 193109 (2006).
- [23] T. Fukuma *et al.*, *Rev. Sci. Instrum.* **76**, 053704 (2005).
- [24] T. Rodriguez and R. Garcia, *Appl. Phys. Lett.* **82**, 4821 (2003).
- [25] R. Garcia, R. Magerle, and R. Perez, *Nature Mater.* **6**, 405 (2007).
- [26] J.K. Hobbs, A.D.L. Humphris, and M.J. Miles, *Macromolecules* **34**, 5508 (2001).

- [27] J. Kumaki, T. Kawauchi, and E. Yashima, *J. Am. Chem. Soc.* **127**, 5788 (2005).
- [28] K. Schmidt-Rohr and H. W. Spiess, *Macromolecules* **24**, 5288 (1991).
- [29] J. Xu *et al.*, *Nature Mater.* **8**, 348 (2009).
- [30] R. Kitamaru, F. Horii, and K. Murayama, *Macromolecules* **19**, 636 (1986).
- [31] B. Wunderlich, *Prog. Polym. Sci.* **28**, 383 (2003).
- [32] J. Kumaki, S. Sakurai, and E. Yashima, *Chem. Soc. Rev.* **38**, 737 (2009).